

pubs.acs.org/Macromolecules Article

Theta Temperature Depression of Mechanically Interlocked Polymers: [2]catenane as a Model Polymer

Hao Guo, Kun Qian, and Mesfin Tsige*



Cite This: Macromolecules 2023, 56, 9164-9174



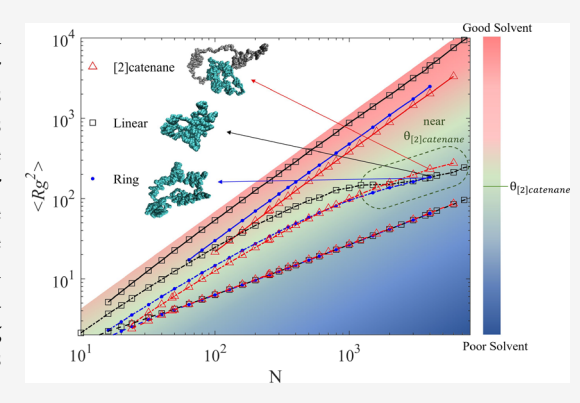
ACCESS I

III Metrics & More

Article Recommendations

SI Supporting Information

ABSTRACT: Polycatenanes have recently attracted considerable attention due to their potential for many applications and as model systems for understanding the role of mechanical interlocking in the physical properties of mechanically interlocked polymers. We used molecular dynamics simulations to investigate the conformational properties of [2]catenane polymers in solution as a function of the solvent quality and molecular weight. We found the θ -temperature of [2]catenane polymers to be depressed compared to their linear and ring counterparts and follow the relationship $\theta_{[2]catenane} < \theta_{ring} < \theta_{linear}$. The conformation of the two rings in [2]catenane is found to be strongly dependent on the solvent quality. In a good solvent, their conformation is similar to that of an analogous free ring polymer, while, in a poor solvent, their conformation significantly deviates from an analogous ring polymer. Furthermore, the thermal blob size ($N_{\rm blob}$) follows the theoretical prediction of the linear relation between $N_{\rm blob}$ and 1/



 v^2 , where v is the excluded volume, and is found to be strongly dependent on polymer topology in a poor solvent condition than in a good solvent condition.

1. INTRODUCTION

Over the past decade, there has been remarkable progress in the synthesis of mechanically interlocked polymers that incorporate mechanical bonds such as polyrotaxanes and polycatenanes. Polycatenanes, a class of polymers that contain two or more interlocked rings, are especially interesting, given the amount of literature devoted to studying the unique properties of isolated ring polymers compared to their linear counterparts. There has been a great deal of interest in ring polymers due to their biological relevance where ring polymers naturally exist in mitochondrial ${\rm DNA}^{1-3}$ and chromatin folding.^{4,5} Furthermore, the absence of free chain ends as well as the inherently topological constraint on ring polymers have made them a model system for understanding the role of chain topology and, as a result, have attracted a lot of attention from theoretical, 6-11 computational, 9,10,12-22 and experimental^{10,23-33} researchers. These unique properties of ring polymers over linear polymers have resulted in a profound effect on their physical properties. 34-38

In addition to possessing all of the unique properties of ring polymers, the components of polycatenanes (i.e., rings) can rotate due to the absence of covalent bonds between them. It is impossible to separate the rings of polycatenanes without breaking any covalent bonds. The mobility of the individual rings within polycatenanes has been attributed to the long list of potential applications of polycatenanes from molecular machines to switchable surfaces.³⁹ Polycatenanes can be used as a model system for understanding the role of mechanical

interlocking in the physical properties of mechanically interlocked polymers. While chemists have achieved notable success in synthesizing various types of polycatenanes, there has been relatively limited focus on exploring their physical properties. ^{36–38,40–42} The majority of research efforts have concentrated on studying their behavior in the melt state, ^{37,38,42} under confinement, ⁴¹ at the liquid—liquid interface, ⁴³ or the self-entanglement within collapsed globule. ⁴⁴ Our objective of the present study is to gain a fundamental understanding of the effect of one catenation point on polymer chain conformation. So, the simplest system to consider is [2] catenane—that is, with just one catenation.

The most convenient systems for studying the properties of macromolecules are polymer solutions. It is safe to say that most of the information that we have now about the properties of macromolecules comes from characterizations realized in solution. A polymer chain exhibits an extended coil structure in a good solvent and collapsed globule in a poor solvent. There is a distinctive intermediate state at which the real chain in solution behaves nearly ideally and follows Gaussian chain

Received: July 31, 2023 Revised: October 17, 2023 Accepted: October 25, 2023 Published: November 9, 2023





statistics at what is known as the θ -point (θ -temperature). Experimentally, the θ -point of a polymer solution system is defined as the temperature at which the osmotic second virial coefficient vanishes. The θ -point is a key concept in polymer physics that has attracted a lot of attention in developing theoretical models including the three-parameter model, 45,40 renormalization group theory, 47-49 and first-order perturbation theory. Identifying the θ -temperature of a given polymer topology—[2] catenane in the present study—is critical in the investigation of the conformation of the polymer chain in a given polymer—solvent system. According to de Gennes and Anisimov, the θ -temperature corresponds to the tricritical point of the thermodynamic system for an infinite long polymer in the description of a critical phenomenon, which separates lines of second-order and first-order transitions.

The basic polymer physics of systems of linear, flexible, uncharged polymers in solution in a wide range of solvent concentrations and qualities can be considered as well understood. The basic physics of uncharged star and ring polymers in dilute solutions can also be considered well understood, and the recent investigation of these systems is mostly focused on semidilute concentrations and on the melt state. In contrast, a similar understanding of poly[n] catenanes, even [2] catenane polymer in dilute solution, has been lacking. Ring and star polymers possess several unique properties in solution compared to their linear counterpart, and a similar investigation of the behavior of poly[n] catenanes in solution is timely, if not overdue. For example, R_g of both star and ring polymers are smaller than their linear counterpart⁵³ (i.e., higher monomer density than linear polymer), and the repulsive forces between segments of a star polymer or a ring polymer at the θ -temperature of a linear polymer are stronger. As a result of this, the topological effect in both star and ring polymers results in a smaller θ -temperature compared to linear polymers. ^{24–28,54–59} The θ -temperature of ring polystyrene in cyclohexane was found to be around 6 K below the θ -temperature of its linear counterpart. However, the θ -temperature depression in star polymers strongly depends on the number of arms and also molecular weight of the arms.⁵⁵

Suzuki et al. 60 using Monte Carlo simulation investigated the scaling behavior of the radius of gyration of [2]catenanes in dilute solution and at different temperatures. They found the Flory scaling exponent, ν , for [2]catenane to be larger than 0.5 at the θ -temperature of the ring polymer. This indicates that the θ -temperature of [2]catenane may be smaller than the θ -temperature of the ring. In this work, using molecular dynamics simulations, we carefully investigated the effect of catenation on the θ -temperature depression of [2]catenane polymers compared to the θ -temperature of ring and linear polymers. Our main goal here is to predict by how much the θ -temperature of [2]catenane is depressed compared to its linear and ring counterparts.

2. METHODS

2.1. Simulation Details. In the present work, the conformational changes of linear, ring, and [2] catenane homopolymers in dilute solution with a wide range of solvent qualities have been studied. The results for linear and ring polymers will be used in explaining the data of [2] catenane polymers. The molecular dynamics (MD) simulations were performed using LAMMPS package 61 with the Kremer–Grest bead spring model. 62 In our simulation, a polymer chain contains N beads, independent of chain topology, representing its total chain length. A [2] catenane polymer chain consists of two identical

interlocked rings with the number of beads in each ring (denoted as N_r) equal to half of the number of beads in the [2]catenane, $N_r = N/2$. The notation of N for the molecular weight of the entire chain and N_r for the molecular weight of each ring in [2]catenane are used throughout the rest of this article. Ring and [2]catenane, sometimes referred to as trivial knot 0_1 and Hopf link 2_1^2 , respectively, were constructed with their contour configuration to avoid knots at the beginning of the simulations. Figure 1 shows a representative

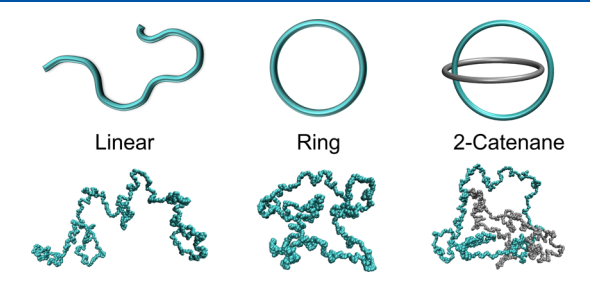


Figure 1. Cartoon representation of linear, ring, and [2]catenane (top row) and representative snapshots of linear, ring, and [2]catenane polymer from simulations (bottom line). The two rings in [2]catenane are colored differently for clarity.

conformation of linear, ring, and [2]catenane polymers. Similar visualization schemes for linear, ring, and [2]catenane polymers are also given in the graphical abstract. The pair interaction between two polymer beads that are not bonded is described by the following shifted Lennard-Jones (LJ) potential.

$$U_{\rm LJ}(r) = \begin{cases} 4\varepsilon \left[\left(\frac{\sigma}{r}\right)^{12} - \left(\frac{\sigma}{r}\right)^6 - \left(\frac{\sigma}{r_c}\right)^{12} + \left(\frac{\sigma}{r_c}\right)^6 \right] \text{ for } r \le r_c \\ 0 \quad \text{otherwise,} \end{cases}$$
 (1)

where r is the distance between two monomers, r_c is the cutoff distance beyond which the LJ interaction is set to be zero, and ε is the depth of the potential well. Bonded beads are connected by finite extensible nonlinear elastic (FENE) bond potential given by 62

$$U_{\text{FENE}} = -\frac{1}{2}kR_0^2 \left[1 - \left(\frac{r}{R_0} \right)^2 \right] + U_{\text{LJ}}(r)$$
 (2)

where the first term is attractive with $k=30\varepsilon/\sigma^2$ and $R_0=1.5\sigma$. The second term is repulsive and is cut off at $r_c=2^{1/6}\sigma$ and shifted. No angle potential has been applied to the polymer chains; the molecules are fully flexible.

Each simulation consists of a single polymer chain in a cubic simulation box with a box side length of about 2.5 times the radius of gyration of the chain in athermal solvent condition to make the system dilute enough. A Langevin thermostat with drag coefficient $\dot{\gamma}=0.01$ was used to ensure a low viscosity of the solution. Integration time steps of 0.01τ and $T=\varepsilon/k_{\rm B}$ were used for all simulations. The shorter molecular weights (N<200) were run for at least 10^{6} τ , the intermediate molecular weights (N<600) were run for at least 10^{7} τ , and the longer molecular weights (N>600) were run for at least 10^{7} τ to achieve a well-equilibrated solution. For comparison, the longest relaxation time of the end-to-end distance vector autocorrelation for a linear polymer of N=6000 is $\sim 10^{5}$ τ ; see Figure S1.

2.2. Implicit Solvent Model. In the Flory—Huggins approach for polymer solution, the effect of solvent on the polymer chain conformation could be integrated out, leading to either attractive or repulsive effective interactions between the monomers or segments of a given polymer chain. Such an effective interaction could be described by the potential of mean force or the local pseudopotential from the microscopic density of the polymer segments. Implicit solvent models are commonly used in the investigation of polymer chain conformation under different solvent and concentration conditions, since they significantly improve computational speed. In this article, the thermodynamic properties of polymer solutions in an

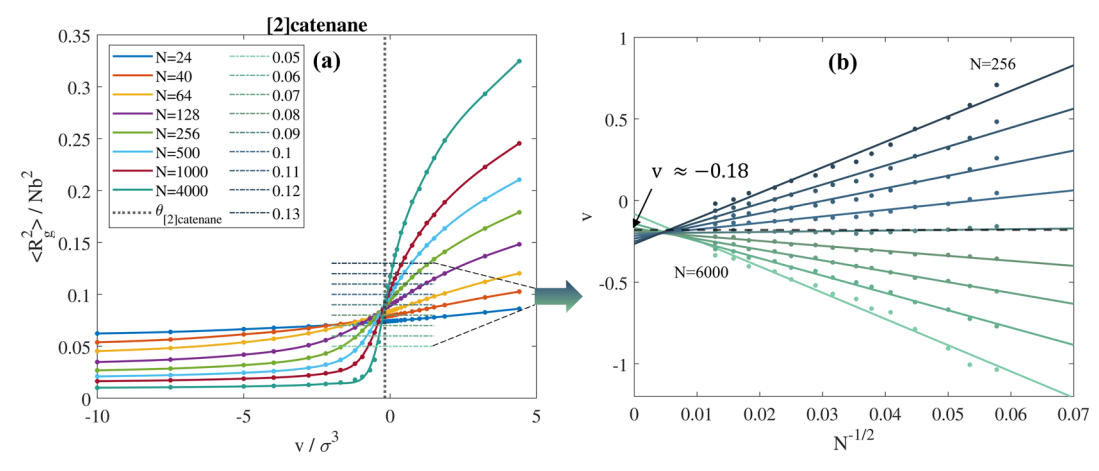


Figure 2. A method to precisely determine the θ -temperature of the ring polymer and [2] catenane polymer: (a) $\langle R_{\rm g}^2 \rangle/Nb^2$ vs v for [2] catenane. Vertical dash line indicates the θ -temperature for analogous linear chain, (b) data points are extracted from the dash-dot horizontal lines of Figure 2a near θ solvent with each color index representing a constant $\langle R_{\rm g}^2 \rangle/Nb^2$ value, the color gradient from light green to dark blue represents the direction of increase in $\langle R_{\rm g}^2 \rangle/Nb^2$ values, and the solid lines are linear fit to the data.

implicit solvent simulation are expressed through what is known as an "effective" monomer—monomer interaction parameter v, referred to as "excluded volume". 53 The excluded volume is a subsum of monomer—monomer, monomer—solvent, and solvent—solvent interactions as well as the entropy of mixing combined into a single parameter. The quality of a given solvent is controlled by the value of v, which is related to the second virial coefficient of monomers A_2 as $v = 2A_2$. 53 The θ -temperature is, in turn, defined as the temperature at which A_2 or v vanishes and a polymer acts like an ideal chain. In implicit-solvent simulations, the excluded volume can be determined through the well-known Mayer f-function: 53

$$\mathbf{v} = \int_0^{r_c} \left(1 - \exp\left[-\frac{U(r)}{k_B T} \right] \right) d^3r \tag{3}$$

where U(r) is the effective monomer–monomer interaction potential given by eq 1 with a cutoff of r_c . In the present work, the magnitude of effective interaction potential was varied by systematically changing r_c from $r_c = 2^{1/6}\sigma$ (athermal solvent) to 3.78 σ (bad solvent) to change the quality of solvent, corresponding to excluded volume values of 4.4 σ 3(athermal solvent) to -10σ 3 (bad solvent), similar to other previous approaches. For simplicity, σ 3 will be dropped when reporting v values in the rest of the article. Increasing v through r_c which is commonly done by the simulation community would correspond to increasing temperature in experiments, which results in a better solvent condition for systems with only upper critical solution temperature (UCST).

3. RESULTS AND DISCUSSION

3.1. Φ-Temperature Determination for Linear, Ring, and [2]catenane Polymers. The most common approach to determining the θ -temperature of a polymer chain in dilute solution is through monitoring the topological size of the polymer chain, characterized by the mean-squared radius of gyration $\langle R_g^2 \rangle$, as a function of N for different solvent qualities. ^{53,65,66} $\langle R_g^2 \rangle / Nb^2$ as a function of solvent quality (as a function of v in the present study) for different values of N is expected to show a common intersection point at the θ -temperature. The value of b we extracted from our simulations ranges between 1.2 and 1.3 σ , and we have used the average value of b=1.25 σ throughout this article. We are aware that the Kuhn length v0 is expected to vary with solvent quality, but we could not extract any meaningful dependence of v0 as a function of excluded volume from our simulation data since the variation seems to be very small.

The $\langle R_g^2 \rangle/Nb^2$ for [2]catenane is shown in Figure 2a and that for linear and ring polymers is shown in Figure S2. As the quality of the solvent changes from good to poor, the longer chains show a transition from an expanded coil state to a collapsed globule state, commonly known as the coil–globule transition. The transition point is identified as the ideal coil state corresponding to the θ -solvent or θ -temperature for infinite chain length, and $\langle R_g^2 \rangle/Nb^2$ is independent of molecular weight. In Figure 2a, the intersection for high molecular weights is around v \approx -0.16, which can be considered as a first estimate of the θ -temperature. To determine the transition point more precisely, the common approach is to extrapolate the simulation data to infinite molecular weight, ⁶⁶ as described below.

A single polymer chain immersed in a bulk solvent obeys the scaling relationship of $R_g \sim v^{2\nu-1}N^{\nu}$, where v is the excluded volume and ν is the Flory exponent ($\nu = 3/5$ in good solvent, ν = 1/2 in θ -solvent, and ν = 1/3 in poor solvent).⁵³ From this, we get the following general relationship for all solvent conditions: $R_{\sigma}^2/N \sim (vN^{1/2})^{4\nu-2}$. Note that |v| should be considered when dealing with poor solvent conditions or when v is negative. The R_{σ}^2/Nb^2 vs $vN^{1/2}$ for [2] catenane is shown in Figure S3 and clearly shows two master curves representing the good solvent and poor solvent regions. We noticed that very poor solvent conditions deviate from the master curve, and we have avoided including those excluded volume values in extracting the θ -temperature. Each of the horizontal dotted lines in Figure 2a represents a constant $vN^{1/2}$ relationship. Collecting the intersection points of each of the lines with the curves results in several straight lines of v versus $N^{-1/2}$ relationships with the slope of each line being proportional to the R_g^2/N value of the corresponding dotted line. The extracted v vs $N^{-1/2}$ relationships from Figure 2a are shown in Figure 2b. The benefit is that these straight lines, if extrapolated to high molecular weight, intersect at the θ temperature. The straight lines in Figure 2b represent the extrapolation to the $N \to \infty$. Note that, as was observed in other previous similar extrapolations,66 the different lines do not intersect at the expected $N^{-1/2} = 0$ due to the finiteness of the chains. The extrapolation to high molecular weight results in $v_{[2]catenane}^{\theta} = -0.18$, close to what we predicted above from Figure 2a. Applying the same extrapolation approach to linear

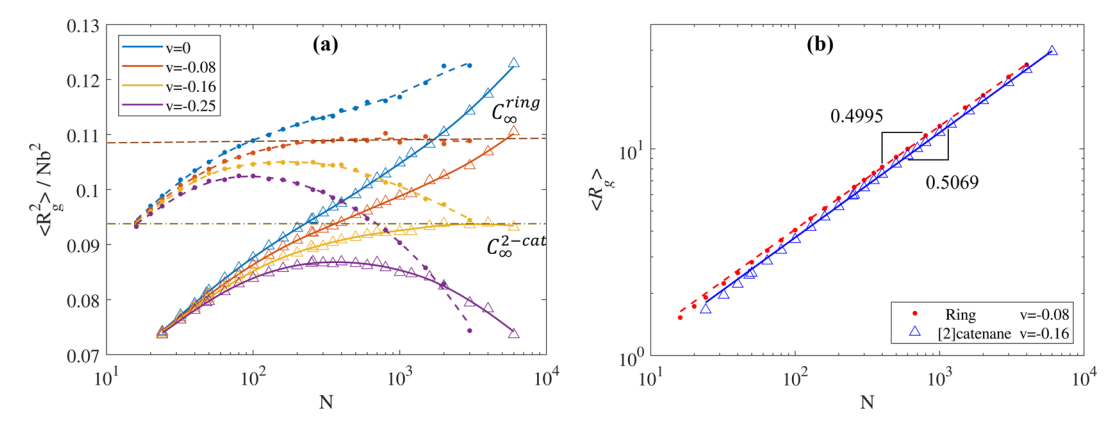


Figure 3. (a) $\langle R_g^2 \rangle / Nb^2$ vs N for ring (filled dots with dash lines) and [2]catenane (empty triangles with solid lines) near θ solvent, (b) $\langle R_g \rangle$ vs N scaling plot at θ solvent for ring (red dots with dash line) and at θ solvent for [2]catenane (blue triangle with a solid line) in double log-scale, lines represent a linear fitting in log-scale, and Flory scaling exponents at the predicted θ solvent values are also shown.

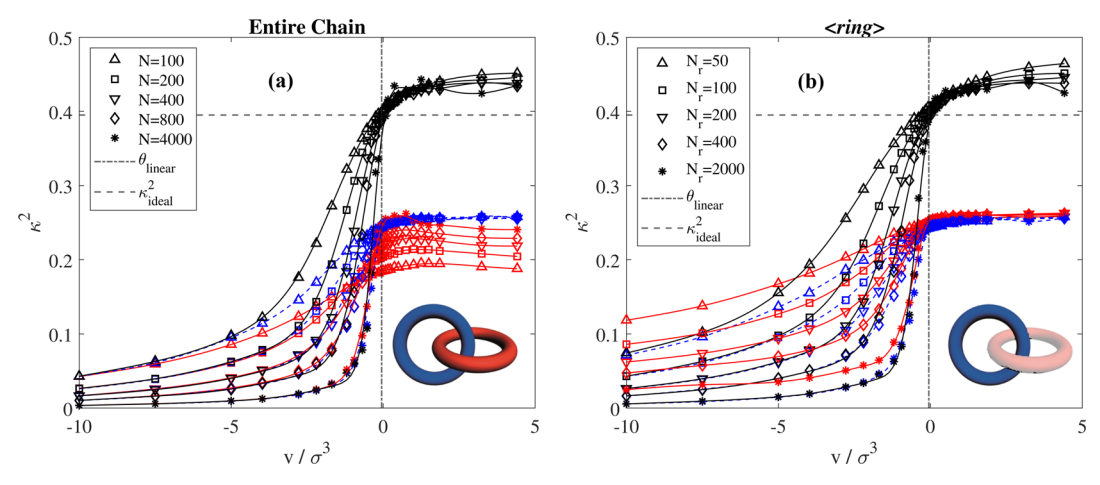


Figure 4. (a) Anisotropy κ^2 for linear (black symbols), ring (blue symbols), and entire chain of [2] catenane (red symbols) as a function of excluded volume. (b) Anisotropy κ^2 for linear, ring, and average of rings in [2] catenane ($\langle \text{ring} \rangle$) shown in red symbols as a function of excluded volume, where the chain length N of linear and ring is half of [2] catenane, $N_{\text{linear}} = N_{\text{ring}} = N_{r}$, which is the chain length of the rings in the [2] catenane. The legend provides a listing of various symbols used to represent the various chain lengths. A vertical gray dash-dot line indicates the θ solvent value for the linear chain. Horizontal dashed lines represent the value for an ideal chain.

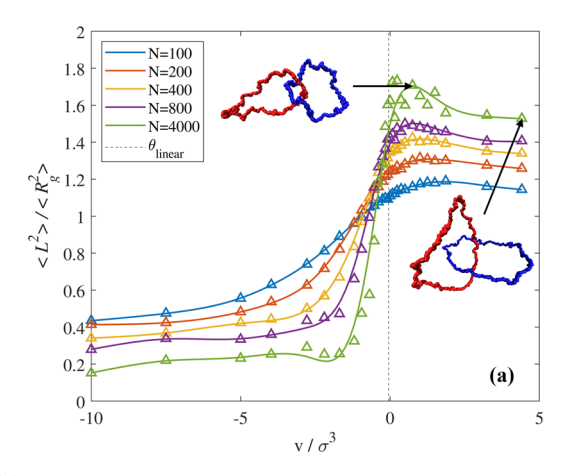
and ring polymers results in $v_{linear}^{\theta} = -0.05$ and $v_{ring}^{\theta} = -0.08$. Since a decrease in v means a decrease in T, a lower v^{θ} should correspond to a lower θ -temperature. On this basis, it is straightforward to conclude that the catenation constraint in [2] catenane significantly reduces its θ -temperature compared to its linear and ring counterparts. Given that the θ temperature depression in ring polystyrene in cyclohexane was found to be around 6 K, 25 we expect the θ -temperature depression in [2]catenane polystyrene compared to ring polystyrene in cyclohexane to be more than 6 K. However, our results contradict that of Dehaghani et al., 36 who concluded that the θ -temperature of poly[n] catenane is greater than the θ -temperature of ring polymers. There is, however, a big difference in the type of catenated polymers investigated in their work and our work. They investigated poly[n] catenanes with the number of beads in the rings of the poly [n] catenane fixed to 32 and varied the number of rings, n, from 32 to 128, while in our case, we fixed n = 2 and varied the number of beads in the two rings from 12 to 3000. Therefore, future systematic investigation is warranted to determine the dependence of the θ -temperature of poly[n]catenane on the number of rings, n. We note in passing that the extrapolated $\mathbf{v}_{\text{linear}}^{\theta}$ is not zero and will be discussed in future work in the

context of the bond energy contribution to the Mayer ffunction of eq 3.

At the θ -temperature, R_g^2/Nb^2 should converge to the well-known Flory characteristic ratio C_∞ at large values of N, and this is confirmed in Figure 3a for both ring and [2]catenane. R_g^2/Nb^2 diverges from this characteristic ratio in good and poor solvent conditions, as also shown in this figure. Furthermore, Figure 3b shows the Flory exponent $\nu \approx 0.5$ for the ring and [2]catenane at their predicted θ -temperatures.

From a fundamental point of view, it is also interesting to do a similar analysis for the two rings in [2]catenane. Since the two rings are of identical chain length ($N_{\rm r}=N/2$ where N is the molecular weight of the whole [2]catenane), we took the average $R_{\rm g}$ of the two rings (denoted as $\langle {\rm ring} \rangle$) for their θ -temperature analysis. The θ -temperature of the rings determined from extrapolation of the ${\rm v}N^{1/2}$ relationship to infinite molecular weight is ${\rm v}^{\theta}_{\langle {\rm ring} \rangle} \approx -0.12$, which is depressed compared to the isolated ring but higher than for [2]catenane. Our results demonstrate the effect of topological constraints on the θ -temperature of polymer chains and can be summarized as $\theta_{\rm [2]catenane} < \theta_{\langle {\rm ring} \rangle} < \theta_{\rm ring} < \theta_{\rm linear}$.

3.2. Effect of Chain Topology on Polymer Chain Conformation. Another useful quantification of polymer



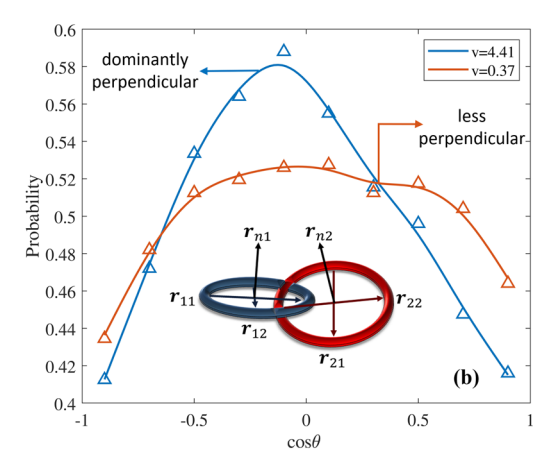


Figure 5. (a) Mean-squared center-to-center distance of the two interlocked rings normalized by the mean-squared radius of gyration of [2] catenane, $\langle L^2 \rangle / \langle R_g^2 \rangle$. The inset snapshots are the visualization of [2] catenane with N=4000 at v=0.37 (less perpendicular orientation) and v=4.4 (dominantly perpendicular orientation). (b) Time-average probability distribution of the angle between the planes of the two interlocked rings for N=4000 at v=0.37 (orange) and 4.4 (blue). The angles are calculated based on the normal vectors r_{n1} and r_{n2} shown in the inset cartoon.

conformation is through monitoring the shape of the polymer chain under different solvent conditions. The conformational change of polymer chains can be captured by the anisotropy (κ^2) model defined as

$$\kappa^{2} \stackrel{\text{def}}{=} \frac{3}{2} \frac{\lambda_{1}^{4} + \lambda_{2}^{4} + \lambda_{3}^{4}}{(\lambda_{1}^{2} + \lambda_{2}^{2} + \lambda_{3}^{2})^{2}} - \frac{1}{2}$$
 (4)

where λ_1^2 , λ_2^2 , and λ_3^2 are the three eigenvalues of the gyration tensor and $0 \le \kappa^2 \le 1$. $\kappa^2 = 0$ corresponds to a perfect sphere and $\kappa^2 = 1$ corresponds to a fully stretched chain. The anisotropy κ^2 for linear, ring, and [2]catenane for different chain lengths and as a function of solvent quality, v, are shown in Figure 4. In all cases, we see the coil-globule transition happening around $v \approx 0$ and the transition becoming sharp as the molecular weight increases. The horizontal dash line indicates the anisotropy for the ideal random walk^{67,68} κ^2 = 0.39, which is around the coil-globule transition region. For the case of linear and ring, κ^2 shows a strong dependence on molecular weight in poor solvent conditions, while no strong dependence on molecular weight is observed in good solvent conditions. For the case of the entire chain of [2]catenane, Figure 4a, κ^2 shows a strong dependence on molecular weight in all solvent conditions. However, the dependence on molecular weight for all cases disappears at high molecular weight; see Figure S4 for the [2]catenane case in the high molecular weight range. At high molecular weight, $\kappa^2 \approx 0$ under poor solvent conditions for all three cases is expected for a spherical globule conformation and does not depend on polymer topology. Under good solvent conditions, the anisotropy is very high for the case of linear chains ($\kappa^2 \approx$ 0.45), while the difference between ring and [2]catenane anisotropies is not significant at high molecular weight ($\kappa^2 \approx$ 0.25 for ring and $\kappa^2 \approx 0.24$ for [2]catenane).

The average anisotropy of the two rings of the [2]catenane (denoted by $\kappa^2_{\langle {\rm ring} \rangle}$ in Figure 4b) shows very interesting behavior. In a good solvent, the anisotropy of the two rings in [2]catenane is the same as that of a free ring. However, in a poor solvent, the $\kappa^2_{\langle {\rm ring} \rangle}$ is much larger than that of κ^2 of free ring polymers with analogous molecular weight. The catenation topology inhibits the rings in [2]catenane from forming a spherical globular morphology.

Intrigued by the maximum κ^2 value observed around v = 0.37 for [2]catenane at high molecular weights, see Figure 4a for the case of N = 4000, we investigated how the two rings in [2] catenane pack relative to each other as a function of solvent quality. The center-to-center distance between the two rings is found to be an important parameter in understanding the solvent quality dependence of the anisotropy, κ^2 , of [2]catenane. 60 Figure 5a shows the mean-squared center-to-center distance of the two interlocked rings, $\langle L^2 \rangle$, normalized by the average radius of gyration of the whole [2] catenane $(\langle R_a^2 \rangle)$. The $\langle L^2 \rangle / \langle R_{\sigma}^2 \rangle$ curve shows a similar behavior as κ^2 with a peak around v \approx 0.37. The $\langle L^2 \rangle$ and $\langle R_g^2 \rangle$ for different chain lengths and as a function of v are shown in Figure S5. The centers of the two rings, $\langle L^2 \rangle$, are very close to each other in poor solvent conditions (in the globule) and start to significantly move apart near the θ -temperature. While both $\langle L^2 \rangle$ and $\langle R_{\sigma}^2 \rangle$ show monotonically increasing behavior with increasing v in a good solvent region (see Figure S5), the $\langle L^2 \rangle / \langle R_{\sigma}^2 \rangle$ plateaus at high solvent qualities.

Furthermore, to better understand the conformation of the two interlocked rings, their relative orientation is investigated by computing the angle between the two normal vectors of the rings, r_{n1} and r_{n2} , as shown in the inset of Figure 5b. The probability distributions of the angles between the two normal vectors for N = 4000 at v = 0.37 and v = 4.4 are shown in Figure 5b. In a good solvent, we observe that the two rings adopt different relative orientations where a less perpendicular orientation of the rings is observed around v = 0.37, as shown in the left side inset in Figure 5a, which maximizes the $\langle L^2 \rangle /$ $\langle R_{\sigma}^2 \rangle$. This orientation also maximizes the anisotropy, κ^2 , of [2] catenane as shown in Figure 4a. With further increase in solvent quality, the orientation of the two rings manifests a dominantly perpendicular orientation as also shown on the right side inset of Figure 5a and that results in a slight decrease in the $\langle L^2 \rangle / \langle R_\sigma^2 \rangle$ and also in the anisotropy. In the plateau region, the $\langle L^2 \rangle / \langle R_g^2 \rangle$ values for [2] catenane converges to 1.5 at high molecular weights, confirming the theoretical prediction. 60 Furthermore, an early investigation by Pakula and Jeszka 69 also observed an increase in $\langle L^2 \rangle / \langle R_g^2 \rangle$ in good solvent within the low molecular weight range they investigated.

Given that the center-to-center distance and orientation of the two rings strongly depend on solvent quality, it will be

interesting to investigate how the conformations of the two rings change as a function of solvent quality compared to their ring counterpart. Figure 6 shows the ratio of the average

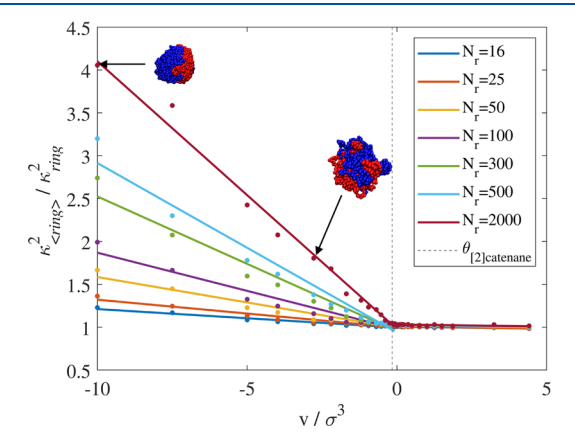


Figure 6. Ratio between the average anisotropy of the two rings of [2] catenane, $\kappa_{(\text{ring})}^2$, and the anisotropy of ring polymer, κ_{ring}^2 , with the same chain length (N_r) as the rings of the [2] catenane. The dash vertical line represents the $\mathbf{v}_{[2]\text{catenane}}^{\theta} = -0.18$. The inset snapshots represent [2] catenane (each ring is represented by different color for clarity) of N = 4000 at $\mathbf{v} = -10$ (nonsolvent) and $\mathbf{v} = -2.8$ (poor solvent).

anisotropy of the two rings of the [2] catenane polymer, $\kappa_{(\text{ring})}^2$, to the anisotropy of the ring polymer, κ_{ring}^2 , as a function of solvent quality. We clearly see two regions separated by the θ solvent condition shown by the vertical dashed line. In a good solvent, the coil conformation of the two rings in [2] catenane is similar to that of ring polymer and hence the anisotropy ratio is about 1. In a poor solvent (globular conformation), the two rings of [2] catenane are more anisotropic than their ring counterpart. In this globular conformation, the two rings tend to be on different sides of the bigger spherical [2]catenane conformation; see the inset snapshot in Figure 6 at a very poor solvent value of v = -10, making the individual rings less spherical than a free ring polymer. This asymmetry decreases as the solvent quality increases toward the θ -solvent condition. However, great care has to be taken in interpreting the dependence of $\kappa_{(\text{ring})}^2/\kappa_{\text{ring}}^2$ on molecular weight since both $\kappa_{(\text{ring})}^2$ and κ_{ring}^2 decrease with an increase in molecular weight (see Figure 4) in poor solvent conditions and tend to go to zero at very high molecular weights.

From our discussion so far, it might seem that the two rings in the [2]catenane have identical conformations under all solvent conditions. That is true when we consider their time average conformation properties, but we observed that they actually display significant conformational differences at any given time. One parameter we investigated is the long-time average difference between the radius of gyration of the two rings as a function of solvent quality. Since the difference in radius of gyration (R_{σ}) between the two rings fluctuates between plus and minus values as a function of time, we consider its absolute value. Figure 7 shows the time-average percentage difference in R_g of the two rings with respect to the ring with the smaller R_g . We clearly see a strong dependence on solvent quality where the difference in R_g of the two rings near θ -solvent could be as high as 20% at the highest molecular weight we studied and slightly decreasing but staying high in good solvent conditions. The peak near the θ -solvent is correlated to the change in the orientation of the two rings.

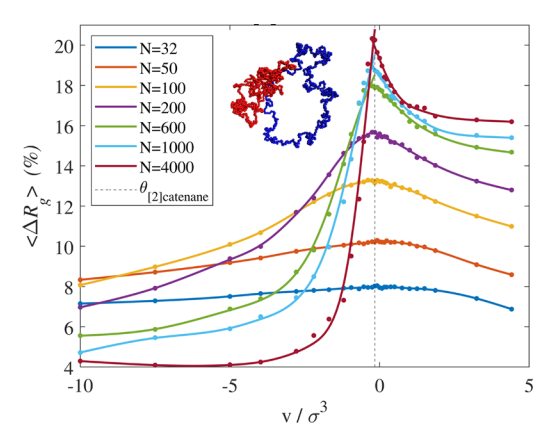


Figure 7. Time-averaged absolute percentage difference in $R_{\rm g}$ between the two rings in [2]catenane as a function of solvent quality, v. The inset snapshot represents the difference in ring size for [2]catenane of N=4000 in θ solvent. Solid lines indicate spline fitting of data points in good and poor solvent conditions. Dash vertical lines represent the $v_{\rm [2]catenane}^{\theta}=-0.18$.

3.3. *g*-Factor for [2]catenane. One important question that we have not addressed to this point is the scaling relation of the mean squared radius of gyration, $\langle R_g^2 \rangle$, of [2]catenane as a function of the molecular weight and solvent quality. Figure 8 is a compilation of all of the [2]catenane and ring $\langle R_g^2 \rangle$ obtained in the present investigation. Apart from a shift in the θ -temperature to a lower value, the $\langle R_g^2 \rangle$ of [2]catenane is found to have a scaling relation similar to that of its linear and ring counterparts in both poor and good solvent conditions. It is then customary to consider the *g*-factor (or contraction factor) of [2]catenane compared to its linear counterparts given by

$$g = \frac{\langle R_g^2 \rangle_{\text{[2]catenane}}}{\langle R_g^2 \rangle_{\text{linear}}} I_N \tag{5}$$

where N is the total chain length of the [2] catenane and its linear counterpart. All of the g-factor values for [2] catenane are presented in Figure 9a. The g-factor for the ring polymer is shown in Figure 9b for comparison. The g-factor for the rings of the [2] catenane (computed using the average $\langle R_g^2 \rangle$ of the two rings) compared to their isolated ring and linear counterparts are shown in Figure S7a,b, respectively. At high molecular weights and good solvent conditions for both [2] catenane and linear polymer, the g-factor values are mainly between 0.4 and 0.46, considerably smaller than for the ring counterparts, which are between 0.5 and 0.55. The g-factor values for ring polymer are consistent with previous studies. 10,21,22,29,70 The data in Figure S7 clearly demonstrate that the size of a ring topologically constrained to another ring is more swollen compared with isolated rings as also pointed out by others.

We observe several interesting behaviors in the dependence of the g-factor on chain molecular weight for both ring and [2] catenane under poor solvent conditions. The g-factor strongly depends on molecular weight and the degree of poor solvent condition; in general, increasing nonlinearly from below 0.5 to around 1 for the case of [2] catenane and from around 0.6 to around 1 for the case of the ring with increasing molecular weight. In order to understand this, we analyzed the bead number density profile, $\phi(r)$, as a function of distance from the chain's center of mass for linear, ring, and

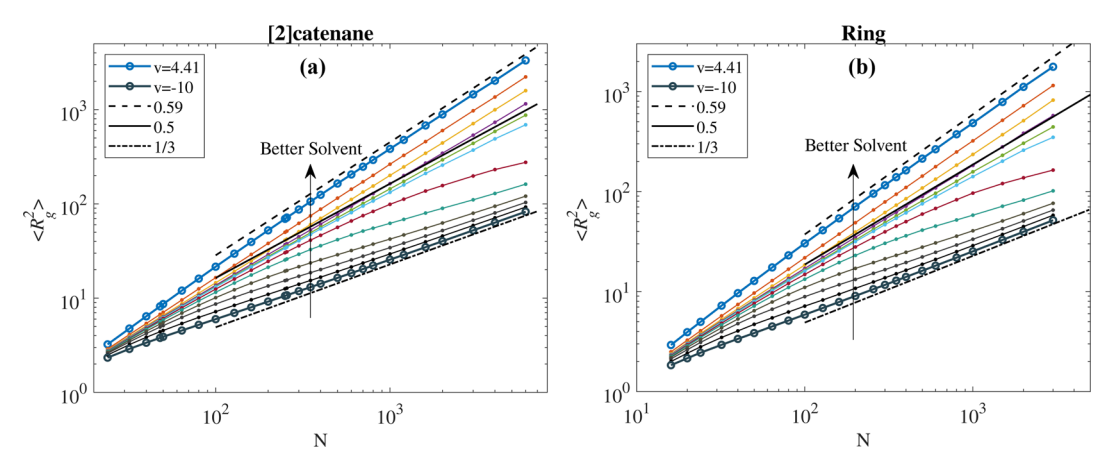


Figure 8. $\langle R_g^2 \rangle$ as a function of N in varying solvent qualities for (a) [2] catenane and (b) the ring polymer. Solvent qualities are shown in the same color index where the best (athermal solvent) and the worst (nonsolvent) are shown as the blue and livid lines with open circles, respectively. The rest of the solvent conditions are represented by different colors and filled circles. The black dash lines, solid lines, and dash-dot lines represent the Flory scaling exponent of 0.59 in a good solvent, 0.5 in a theta solvent, and 1/3 in a poor solvent, respectively. The $\langle R_g^2 \rangle$ for the linear case is shown in Figure S6.

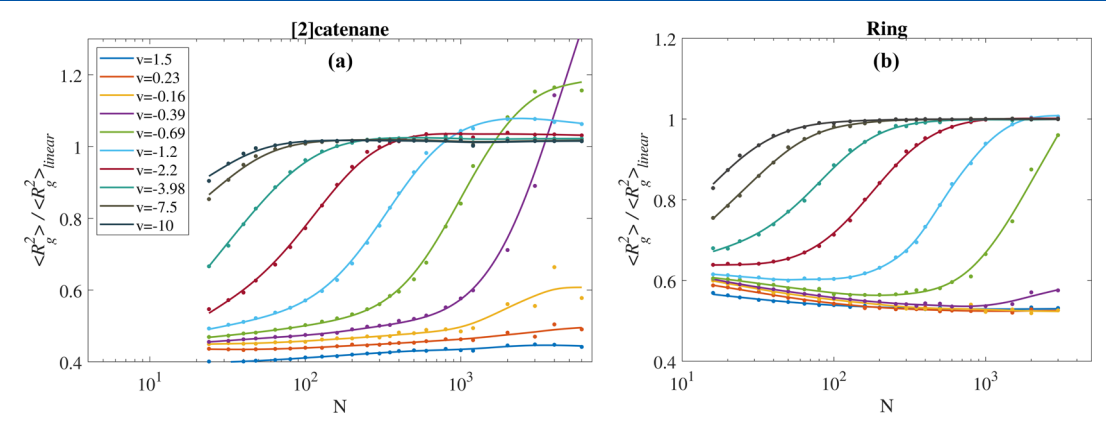


Figure 9. g-factor, $\langle R_g^2 \rangle / \langle R_g^2 \rangle_{\text{linear}}$, as a function of entire chain length N in varying solvent qualities for (a) [2] catenane polymer and (b) ring polymer. Solid lines represent spline fits to the data points.

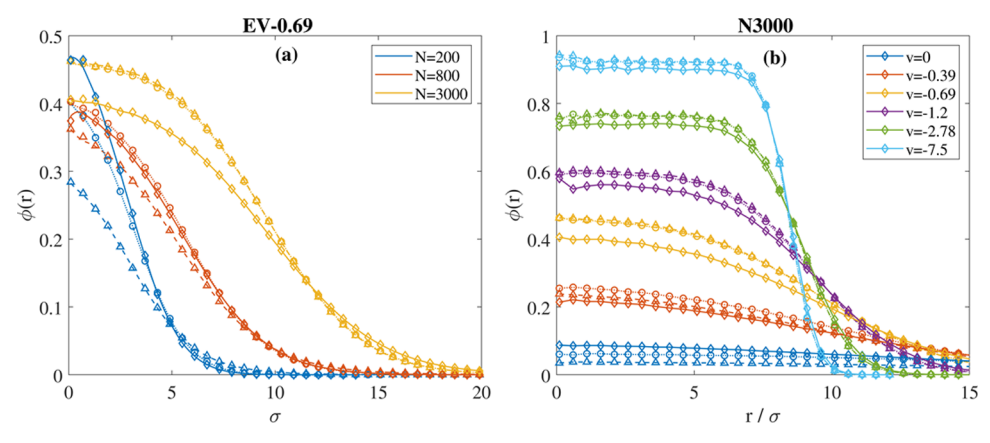


Figure 10. Bead number density profile, $\phi(r)$, as a function of distance from the chain's center of mass for linear (triangles with dash line), ring (empty circles with dotted line), and [2]catenane (empty diamonds with solid line) in poor solvent conditions and one good solvent (v = 4.4, athermal) condition: (a) at v = -0.69 for different chain lengths and (b) at N = 3000 for different poor solvent conditions.

[2] catenane in poor solvent conditions. Figure 10a shows $\phi(r)$ as a function of distance for the three chain topologies at excluded volume v = -0.69 and at different molecular weights. For low molecular weights, the cores of [2] catenane and ring polymers are more dense than their linear polymer counterpart, resulting in a *g*-factor that is well below 1.0. Increasing the

molecular weight of the chains reverses this trend where the core of [2] catenane is less dense (which is larger R_g) than ring and linear polymers, resulting in a g-factor above 1.0. Note that $\phi(r)$ of ring and linear polymers are overlapping at high molecular weight, resulting in a g-factor for the ring of \approx 1.0, as shown in Figure 9b. This observation is valid for all different

poor solvent conditions, as shown in Figure 10b for $\phi(r)$ at high molecular weight of N=3000. $\phi(r)$ for [2]catenane stays below the $\phi(r)$ of the ring and linear polymers for all the poor solvent conditions (Figure 10b), resulting in a g-factor above 1.0, as shown in Figure 9a. Using the bead number density profiles, we computed the average core density as a function of N at different poor solvent conditions, and it is shown in Figure 11.

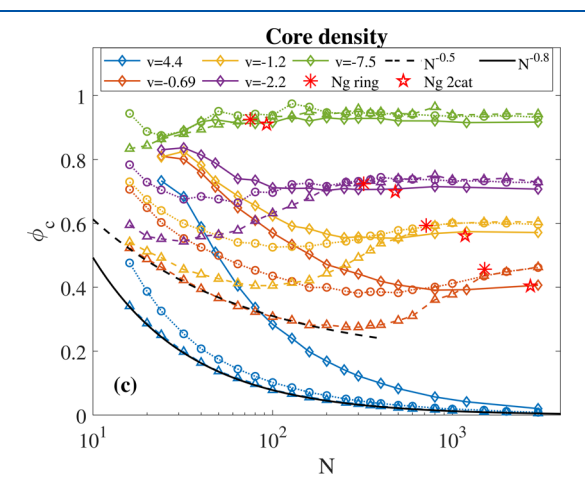


Figure 11. Average core density as a function of chain length in logarithmic scale under selected poor solvent conditions and athermal condition. The black dashed and solid lines represent the relationship of $N^{-0.5}$ and $N^{-0.8}$, respectively.

From Figure 11, the core density in poor solvent conditions initially decreases with an increase in molecular weight for most of the poor solvent conditions except the bad solvent (v = -10) and then fluctuates around a constant value at high molecular weights. The molecular weight range where the core density decreases is strongly dependent on solvent quality and disappears in bad solvent conditions. Assuming each of the beads occupies a volume of $\approx b^3$, the bead number density for a chain within a radius of R_g ($\approx bN^{\nu}$) can be approximated to be $\approx \frac{Nb^3}{(1+N^{\nu})^3} = N^{1-3\nu}$, where ν is the Flory exponent. For an ideal

chain ($\nu = 0.5$), the bead number density of a polymer chain decreases with $N^{-0.5}$, as observed in Figure 11, for low molecular weights (black dash line). This implies that in the low molecular weight range where the core density decreases, the polymer chains behave like an ideal chain. Furthermore, in a globule conformation ($\nu = 1/3$), the bead number density of a polymer chain is independent of molecular weight, as observed in Figure 11, for high molecular weights. Similarly, for polymer chains in coil conformation ($\nu \approx 0.6$), their volume fraction decreases with $N^{-0.8}$, as also shown in Figure 11 for the case of athermal solvent conditions (black solid line). The picture that comes out of this observation is that the effect of the solvent is felt above a certain molecular weight that is strongly dependent on solvent quality, and this finding agrees with the thermal blob idea presented in Section 3.4 below.

In order to gain a deeper insight, we extracted the molecular weight at which the g-factor crosses (for [2]catenane) or reaches (for the ring) 1.0 for each of the different poor solvent qualities we simulated, and the results are shown in Figure 11 by red star symbols. These values (referred to hereafter as N_{σ}) are in the globule region where the bead number density is independent of molecular weight. For $N > N_g$, ring polymers behave like linear polymers with the g-factor around 1.0, while the g-factor for [2]catenane is above 1.0 because the core density of [2] catenane is smaller than those of linear and ring polymers. While the effect of chain topology for ring polymers persists up to $N < N_g$, the effect of the mechanical bond in [2]catenane persists throughout the chain length range we investigated $(N \gg N_{\rm g})$ and demonstrates the strong effect mechanical bonds have on the chain conformation of catenated polymers and hence resulting in the large drop in the θ temperature for [2]catenane compared to isolated ring polymers. In special cases such as close to the θ -solvent region of [2]catenane, which is a poor solvent region for a linear polymer, the g-factor of [2] catenane is found to be significantly larger than 1 at high molecular weights as shown, for example, for v = -0.39, confirming that the linear polymer is more collapsed than [2]catenane.

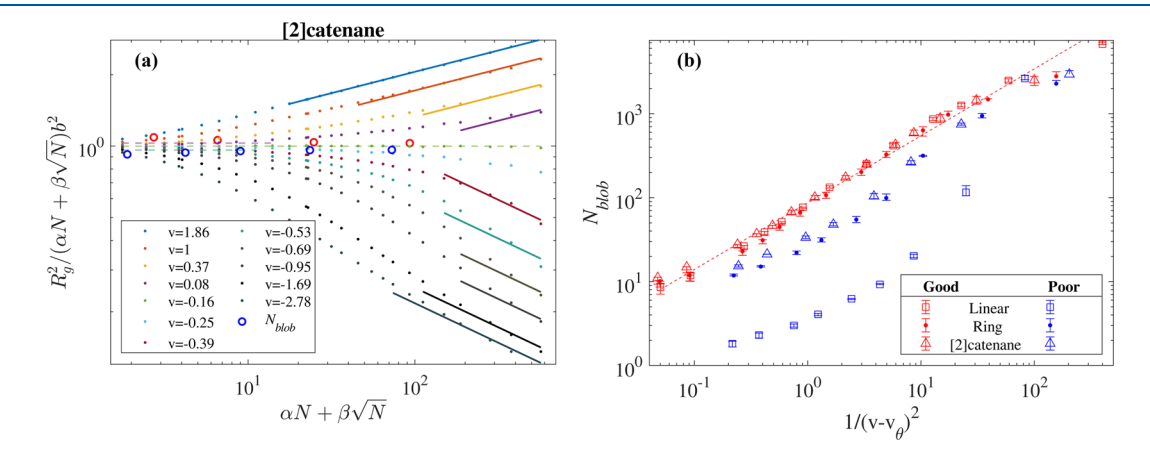


Figure 12. (a) $R_g^2/(\alpha N + \beta \sqrt{N})b^2$ vs $(\alpha N + \beta \sqrt{N})$ for [2]catenane under selected solvent conditions. Two different regimes are identified, and the dashed lines represent the regime with zero slope. The solid lines represent the region with a slope of 0.18 (good solvent cases) and a slope of -1/3 (poor solvent cases). The thermal blob, N_{blob} , for each solvent quality is represented by red open circles (good solvent cases) and blue open circles (poor solvent cases). (b) Thermal blob N_{blob} extracted using the same method for linear (asterisk), ring (solid circles), and [2]catenane (open triangles) vs $1/v'^2$ where $v' = v - v_\theta$ (shifted by the corresponding q-solvent quality for linear or ring or [2]catenane). The red and blue colors represent the results in good and poor solvent conditions, respectively.

3.4. Effect of Chain Topology on Thermal Blob Size.

The thermal blob represents a length scale at which excluded volume interactions become comparable to the thermal energy. It is thus intuitive to expect the thermal blob size to decrease with increasing excluded volume interaction, v. If $N_{\rm blob}$ represents the number of beads in a thermal blob, then a polymer chain in a given solvent quality with $N < N_{\rm blob}$ will behave as a nearly ideal chain. However, for $N > N_{\rm blob}$, the polymer chain collapses to a globule in a poor solvent or will swell in a good solvent. In Figure 8, we clearly see the transition from ideal chain behavior to a globule for most of the poor solvent conditions since it is easy to notice with the naked eye the change of slope from around 1.0 to around 0.6 under poor solvent conditions, which is not the case for good solvent conditions where the change of slope is from around 1.0 to around 1.2.

Note that near θ -temperature and in the low molecular weight limit, large deviations from Gaussian chain properties have been reported, 65 and the R_g^2 deviates from the ideal chain behavior could have the square root correction format $R_a^2 \approx (\alpha N + \beta \sqrt{N}) b^{263,72}$ or the logarithmic correction $R_g^2 \approx N b^2 \left[1 - \frac{B}{\ln(N/s_0)} \right]^{.65}$ For the logarithmic correction model, B = 37/363, -37/363 and $1.9/(44\pi)$ are reported by mean-field theory methods.⁶⁵ Unfortunately, the logarithmic correction does not fit our data in the low and intermediate molecular weight range (see Figure S8), in which we are interested in extracting thermal blob size. Similar results have been reported by Grassberger and Hegger. 73 The square root correction better describes our simulation data than the logarithmic correction, and we used the square root correction for extracting thermal blob sizes as a function of the solvent quality. Plotting $R_g^2/(\alpha N + \beta \sqrt{N})b^2$ using the square root correction as a function of $\alpha N + \beta \sqrt{N}$, as shown in Figure 12a, for [2]catenane (see Figure S10 for linear and ring) separates the ideal chain region from the globule or swollen region with chosen α and β parameters shown in Table S1 and Figure S9. For a given solvent quality and for $N < N_{blob}$, this plot is a constant line with slope of around zero. The slope then slowly changes to around 0.18 in a good solvent or to around -1/3 in a poor solvent for $N > N_{blob}$, as shown in the figure. Under poor solvent conditions, there is a transition region before the slope converges to -1/3. The thermal blob size for each solvent quality is obtained as the intersection between these two lines. The thermal blob size (N_{blob}) estimated using this approach for different solvent qualities is also shown in Figure 12a as large open circles (colored in blue in poor solvent and in red under good solvent conditions).

The number of beads in a thermal blob $(N_{\rm blob})$ is, in general, expressed as a function of excluded volume through $N_{\rm blob} \approx b^6/{\rm v}^2,^{51,53}$ where b is the Kuhn length. $N_{\rm blob}$ as a function of $1/{\rm v'}^2$ for linear, ring, and [2]catenane is shown in Figure 12b where ${\rm v'} = {\rm v} - {\rm v}_\theta$ (shifted by the corresponding θ -solvent for linear or ring or [2]catenane). In good solvent conditions, $N_{\rm blob}$ is independent of chain topology, and a linear relation is observed with a slope of 0.797 \pm 0.02. However, in poor solvent conditions, $N_{\rm blob}$ shows a strong dependence on chain topology with a slope of 1.12 \pm 0.15 for linear, 0.87 \pm 0.12 for ring, and 0.83 \pm 0.11 for [2]catenane. Our results imply that for a given solvent, for example, polystyrene in cyclohexane, $N_{\rm blob}^{\rm [2]catenane} > N_{\rm blob}^{\rm ring} > N_{\rm blob}^{\rm linear}$. Overall and to the best of our knowledge, this is the first investigation that verified the

theoretical prediction of the linear relation between N_{blob} and $1/v^2$.

4. CONCLUSIONS

Molecular dynamics simulations were used to investigate the conformational properties of the [2]catenane polymer under a wide range of solvent qualities and are compared with analogous linear and ring polymers. By using several different methods and a large number of simulations, we can extract the θ -temperature from simulation data in a relatively precise way. Our results demonstrate the effect of topological constraints on the θ -temperature of polymer chains, which follows the relationship of $\theta_{[2]catenane} < \theta_{\langle ring \rangle} < \theta_{ring} < \theta_{linear}$, where $\langle ring \rangle$ represents the average of the two locked rings of [2]catenane. Due to the effect of the mechanical bond, the two linked rings are larger than an isolated ring, resulting in a depression of their θ -temperature compared to an isolated ring. Furthermore, there is a strong tendency for the two linked rings to spatially segregate around the coil-globule transition region, as was shown through the center-to-center distance of the rings, and the magnitude of the segregation increases with the molecular weight of the rings. While the effect of topology in ring polymers becomes negligible above a molecular weight that is strongly dependent on solvent quality as demonstrated through the g-factor, the effect of mechanical bond in the conformation of [2] catenane persists throughout the molecular weight range we investigated. These findings about [2]catenanes seem to correlate well with the large drop in the θ temperature of the [2] catenane compared to that of an isolated

A separate analysis of the two rings in [2] catenane captured their interesting conformational changes that could be different from the conformation of the main [2] catenane depending on the solvent quality. In a good solvent, their conformation is similar to an analogous ring polymer, while, in a poor solvent, their conformation significantly deviates from an analogous ring polymer, displaying high anisotropy. Furthermore, while the two rings on average have comparable radius of gyration in any given solvent, the difference in their radius of gyration as a function of time could reach as high as 20% in a good solvent condition. Their center-to-center distance is also dependent on solvent quality; the rings are pushed apart and manifest a dominantly perpendicular orientation in good solvent conditions

Finally, using the square root correction form for R_g^2 , we were able to extract the thermal blob size at different solvent qualities and for linear, ring, and [2]catenane polymers. The thermal blob size, in general, is found to follow the theoretical prediction of the linear relation between $N_{\rm blob}$ and $1/v^2$, where v is the excluded volume. The thermal blob size is found to be more strongly dependent on polymer topology in poor solvent conditions than in good solvent conditions.

ASSOCIATED CONTENT

Data Availability Statement

Additional information regarding the gyration radius, anisotropy, thermal blob, and comparison between linear and ring analogies are provided in the Supporting Information. All simulation trajectory data that support the findings of this study are available from the corresponding author upon reasonable request.

Supporting Information

The Supporting Information is available free of charge at https://pubs.acs.org/doi/10.1021/acs.macromol.3c01509.

Proof of system equilibration, $\langle R_{\rm g}^2 \rangle / Nb^2$ for linear and ring polymer, anisotropy, $\langle R_{\rm g}^2 \rangle$ scaling, number density profile, averaged core density, and logarithmic and square root models for $\langle R_{\rm g}^2 \rangle$ with corresponding coefficient and the thermal blob size (PDF)

AUTHOR INFORMATION

Corresponding Author

Mesfin Tsige — School of Polymer Science & Polymer Engineering, The University of Akron, Akron, Ohio 44325, United States; ⊙ orcid.org/0000-0002-7540-2050; Email: mtsige@uakron.edu

Authors

Hao Guo — School of Polymer Science & Polymer Engineering, The University of Akron, Akron, Ohio 44325, United States; orcid.org/0000-0002-5649-6346

Kun Qian – School of Polymer Science & Polymer Engineering, The University of Akron, Akron, Ohio 44325, United States

Complete contact information is available at: https://pubs.acs.org/10.1021/acs.macromol.3c01509

Author Contributions

H.G. performed the simulations, collected and performed data analysis, and drafted the initial manuscript. K.Q. contributed to coding assistance for data management and collection. M.T. provided guidance throughout the study, including in the writing of the manuscript.

Notes

The authors declare no competing financial interest.

ACKNOWLEDGMENTS

Authors acknowledge financial support from the National Science Foundation (DMR-1912329 and DMR- 2114640).

REFERENCES

- (1) Sloan, D. B. One Ring to Rule Them All? Genome Sequencing Provides New Insights into the "master Circle" Model of Plant Mitochondrial DNA Structure. *New Phytol.* **2013**, 200 (4), 978–985.
- (2) Kozik, A.; Rowan, B. A.; Lavelle, D.; Berke, L.; Eric Schranz, M.; Michelmore, R. W.; Christensen, A. C. The Alternative Reality of Plant Mitochondrial DNA: One Ring Does Not Rule Them All. *PLoS Genetics* **2019**, *15* (8), No. 1008373.
- (3) Yadav, I.; Al Sulaiman, D.; Soh, B. W.; Doyle, P. S. Phase Transition of Catenated DNA Networks in Poly(Ethylene Glycol) Solutions. ACS Macro Lett. 2021, 10 (11), 1429–1435.
- (4) Halverson, J. D.; Smrek, J.; Kremer, K.; Grosberg, A. Y. From a Melt of Rings to Chromosome Territories: The Role of Topological Constraints in Genome Folding. *Rep. Prog. Phys.* **2014**, *77* (2), 24.
- (5) Jost, D.; Carrivain, P.; Cavalli, G.; Vaillant, C. Modeling Epigenome Folding: Formation and Dynamics of Topologically Associated Chromatin Domains. *Nucleic Acids Res.* **2014**, *42* (15), 9553–9561.
- (6) Prentis, J. J. Spatial Correlations in a Self-Repelling Ring Polymer. J. Chem. Phys. 1982, 76 (3), 1574–1585.
- (7) Grosberg, A. Y. Critical Exponents for Random Knots. *Phys. Rev. Lett.* **2000**, 85 (18), 3858–3861.
- (8) Hirayama, N.; Tsurusaki, K.; Deguchi, T. Linking Probabilities of Off-Lattice Self-Avoiding Polygons and the Effects of Excluded Volume. *J. Phys. A: Math. Theor.* **2009**, *42* (10), No. 105001.

- (9) Uehara, E.; Deguchi, T. Statistical and Hydrodynamic Properties of Topological Polymers for Various Graphs Showing Enhanced Short-Range Correlation. *J. Chem. Phys.* **2016**, *145* (16), 164905.
- (10) Gartner, T. E.; Haque, F. M.; Gomi, A. M.; Grayson, S. M.; Hore, M. J. A.; Jayaraman, A. Scaling Exponent and Effective Interactions in Linear and Cyclic Polymer Solutions: Theory, Simulations, and Experiments. *Macromolecules* **2019**, 52 (12), 4579–4589.
- (11) Douglas, J.; Freed, K. F. Renormalization and the Two-Parameter Theory. 1. *Macromolecules* **1984**, *17* (11), 2344–2354.
- (12) Müller, M.; Wittmer, J. P.; Cates, M. E. Topological Effects in Ring Polymers: A Computer Simulation Study. *Phys. Rev. E: Stat. Phys., Plasmas, Fluids, Relat. Interdiscip. Top.* **1996**, *53* (5), 5063–5074.
- (13) Milchev, A.; Wittmer, J. P.; Landau, D. P. Dynamical Monte Carlo Study of Equilibrium Polymers: Effects of High Density and Ring Formation. *Phys. Rev. E: Stat. Phys., Plasmas, Fluids, Relat. Interdiscip. Top.* **2000**, *61* (3), 2959–2966.
- (14) Wittmer, J. P.; Van Der Schoot, P.; Milchev, A.; Barrat, J. L. Dynamica Monte Carlo Study a Equilibrium Polymers. II. The Role of Rings. *J. Chem. Phys.* **2000**, *113* (16), 6992–7005.
- (15) Müller, M.; Wittmer, J. P.; Cates, M. E. Topological Effects in Ring Polymers. II. Influence of Persistence Length. *Phys. Rev. E: Stat. Phys., Plasmas, Fluids, Relat. Interdisc. Top.* **2000**, *61* (4), 4078–4089.
- (16) Jang, S. S.; Çağin, T.; Goddard, W. A. Effect of Cyclic Chain Architecture on Properties of Dilute Solutions of Polyethylene from Molecular Dynamics Simulations; American Institute of PhysicsAIP, 2003; Vol. 119, pp 1843–1854.
- (17) Suzuki, J.; Takano, A.; Matsushita, Y. The Theta-Temperature Depression Caused by Topological Effect in Ring Polymers Studied by Monte Carlo Simulation. *J. Chem. Phys.* **2011**, *135* (20), 204903.
- (18) Suzuki, J.; Takano, A.; Matsushita, Y. Topological Constraint in Ring Polymers under Theta Conditions Studied by Monte Carlo Simulation. *J. Chem. Phys.* **2013**, *138* (2), 24902.
- (19) Suzuki, J.; Takano, A.; Matsushita, Y. Interactions between Ring Polymers in Dilute Solution Studied by Monte Carlo Simulation. *J. Chem. Phys.* **2015**, *142* (4), No. 044904.
- (20) Chen, Y. D. On the Ring-to-Chain Ratios of Radii of Gyration and Sedimentation Coefficients of Polymers of the Freely Jointed Model: Monte Carlo Calculations and the ε Method. *J. Chem. Phys.* 1983, 78 (8), 5191–5196.
- (21) Zifferer, G.; Preusser, W. Monte Carlo Simulation Studies of the Size and Shape of Ring Polymers. *Macromol. Theory Simul.* **2001**, 10 (5), 397–407.
- (22) Kanaeda, N.; Deguchi, T. Diffusion of a Ring Polymer in Good Solution via the Brownian Dynamics with No Bond Crossing. *J. Phys. A: Math. Theor.* **2008**, *41* (14), No. 145004.
- (23) Roovers, J.; Toporowski, P. M. Synthesis of High Molecular Weight Ring Polystyrenes. *Macromolecules* **1983**, *16* (6), 843–849.
- (24) Roovers, J. DILUTE-SOLUTION PROPERTIES OF RING POLYSTYRENES. J. Polym. Sci., Part A-2 1985, 23 (6), 1117–1126.
- (25) Iwata, K. Evidence of Topological Interaction among Polymers: A 2 of Ring Polymers in the 0-State. *Macromolecules* **1985**, *18* (1), 115–116.
- (26) Tanaka, F. Osmotic Pressure of Ring-Polymer Solutions. J. Chem. Phys. 1987, 87 (7), 4201–4206.
- (27) Iwata, K. θ Temperature of Ring Polymers: Another Evidence of Topological Interaction. *Macromolecules* 1989, 22 (9), 3702–3706.
- (28) McKenna, G. B.; Hostetter, B. J.; Hadjichristidis, N.; Fetters, L. J.; Plazek, D. J. A Study of the Linear Viscoelastic Properties of Cyclic Polystyrenes Using Creep and Recovery Measurements. *Macromolecules* **1989**, 22 (4), 1834–1852.
- (29) Takano, A.; Ohta, Y.; Masuoka, K.; Matsubara, K.; Nakano, T.; Hieno, A.; Itakura, M.; Takahashi, K.; Kinugasa, S.; Kawaguchi, D.; Takahashi, Y.; Matsushita, Y. Radii of Gyration of Ring-Shaped Polystyrenes with High Purity in Dilute Solutions. *Macromolecules* **2012**, 45 (1), 369–373.
- (30) Higgins, J. S.; Dodgson, K.; Semlyen, J. A. Studies of Cyclic and Linear Poly(Dimethyl Siloxanes): 3. Neutron Scattering Measure-

- ments of the Dimensions of Ring and Chain Polymers. *Polymer* 1979, 20 (5), 553-558.
- (31) Ragnetti, M.; Geiser, D.; Höcker, H.; Oberthür, R. C. Small Angle Neutron Scattering (SANS) of Cyclic and Linear Polystyrene in Toluene. *Makromol. Chem.* 1985, 186 (8), 1701–1709.
- (32) Lutz, P.; McKenna, G.; Rempp, P.; Strazielle, C. Solution Properties of Ring-shaped Polystyrenes. *Makromol. Chem., Rapid Commun.* **1986**, 7 (9), 599–605.
- (33) Hadziioannou, G.; Cotts, P. M.; Brinke, G. T.; Han, C. C.; Lutz, P.; Strazielle, C.; Rempp, P.; Kovacs, A. J. Thermodynamic and Hydrodynamic Properties of Dilute Solutions of Cyclic and Linear Polystyrenes. *Macromolecules* **1987**, *20* (3), 493–497.
- (34) Stoddart, J. F. Mechanically Interlocked Molecules (MIMs)—Molecular Shuttles, Switches, and Machines (Nobel Lecture). *Angew. Chem., Int. Ed.* **2017**, *56* (37), 11094–11125.
- (35) Lei, H.; Zhang, J.; Wang, L.; Zhang, G. Dimensional and Shape Properties of a Single Linear Polycatenane: Effect of Catenation Topology. *Polymer* **2021**, *212*, No. 123160.
- (36) Ahmadian Dehaghani, Z.; Chubak, I.; Likos, C. N.; Ejtehadi, M. R. Effects of Topological Constraints on Linked Ring Polymers in Solvents of Varying Quality. *Soft Matter* **2020**, *16* (12), 3029–3038.
- (37) Rauscher, P. M.; Schweizer, K. S.; Rowan, S. J.; De Pablo, J. J. Thermodynamics and Structure of Poly[n]Catenane Melts. *Macromolecules* **2020**, *53* (9), 3390–3408.
- (38) Rauscher, P. M.; Schweizer, K. S.; Rowan, S. J.; de Pablo, J. J. Dynamics of Poly[n]Catenane Melts. *J. Chem. Phys.* **2020**, *152* (21), 214901.
- (39) Wu, Q.; Rauscher, P. M.; Lang, X.; Wojtecki, R. J.; De Pablo, J. J.; Hore, M. J. A.; Rowan, S. J. Poly[n]Catenanes: Synthesis of Molecular Interlocked Chains. *Science* **2017**, 358 (6369), 1434–1439.
- (40) Zhou, K.; Lu, Y.; Li, J.; Shen, L.; Zhang, G.; Xie, Z.; Wu, C. The Coil-to-Globule-to-Coil Transition of Linear Polymer Chains in Dilute Aqueous Solutions: Effect of Intrachain Hydrogen Bonding. *Macromolecules* **2008**, *41* (22), 8927–8931.
- (41) Polles, G.; Orlandini, E.; Micheletti, C. Optimal Self-Assembly of Linked Constructs and Catenanes via Spatial Confinement. *ACS Macro Lett.* **2016**, *5* (8), 931–935.
- (42) Rauscher, P. M.; Rowan, S. J.; De Pablo, J. J. Topological Effects in Isolated Poly[n]Catenanes: Molecular Dynamics Simulations and Rouse Mode Analysis. *ACS Macro Lett.* **2018**, *7* (8), 938–943.
- (43) Shandiz, S. A.; Leuty, G. M.; Guo, H.; Mokarizadeh, A. H.; Maia, J. M.; Tsige, M. Structure and Thermodynamics of Linear, Ring, and Catenane Polymers in Solutions and at Liquid—Liquid Interfaces. *Langmuir* **2023**, *39* (20), 7154—7166.
- (44) Dehaghani, Z. A.; Chiarantoni, P.; Micheletti, C. Topological Entanglement of Linear Catenanes: Knots and Threadings. ACS Macro Lett. 2023, 12 (9), 1231–1236.
- (45) Yamakawa, H. Three-Parameter Theory of Dilute Polymer Solutions. J. Chem. Phys. 1966, 45 (7), 2606–2617.
- (46) Yamakawa, H. Hiromi Yamakawa Modern Theory of Polymer Solutions, 2001; pp 1-434.
- (47) Stephen, M. J. Collapse of a Polymer Chain. *Phys. Lett. A* **1975**, 53 (5), 363–364.
- (48) Duplantier, B. Lagrangian Tricritical Theory of Polymer Chain Solutions Near the Theta -Point *J. Phys.* 1982, 43, 991–1019 DOI: 10.1051/jphys:01982004307099100.
- (49) Duplantier, B. Tricritical Polymer Chains in or below Three Dimensions. *EPL* **1986**, *1* (10), 491–498.
- (50) Zhang, P.; Alsaifi, N. M.; Wang, Z. G. Revisiting the Θ Point. *Macromolecules* **2020**, 53 (23), 10409–10420.
- (51) de Gennes, P. G. Scaling Concepts in Polymer Physics; Cornell University Press, 1979.
- (52) Anisimov, M. A.; Agayan, V. A.; Gorodetskil, E. E. Scaling and Crossover to Tricriticality in Polymer Solutions. *JETP Lett.* **2000**, 72 (11), 578–582.
- (53) Rubinstein, M.; Colby, R. H. Polymer Physics; Oxford University Press, 2003.

- (54) Noda, I.; Horikawa, T.; Kato, T.; Fujimoto, T.; Nagasawa, M. Solution Properties of Comb-Shaped Polystyrenes. *Macromolecules* **1970**, 3 (6), 795–799.
- (55) Roovers, J. E. L.; Bywater, S. Preparation of Six-Branched Polystyrene. Thermodynamic and Hydrodynamic Properties of Fourand Six-Branched Star Polystyrenes. *Macromolecules* **1974**, *7* (4), 443–449.
- (56) Khasat, N.; Pennisi, R. W.; Hadjichristidis, N.; Fetters, L. J. Dilute Solution Behavior of Asymmetric Three-Arm and Regular Three- and Twelve-Arm Polystyrene Stars. *Macromolecules* **1988**, 21 (4), 1100–1106.
- (57) Bruns, W.; Carl, W. Relations between Averaged Configurational Properties of Linear and Starlike Polymer Models at the θ Temperature. *Macromolecules* **1991**, 24 (1), 209–212.
- (58) Li, B.; Sun, Z.; An, L.; Wang, Z. G. The Scaling Behavior of the Second Virial Coefficient of Linear and Ring Polymer. *Sci. China Chem.* **2016**, *59* (5), *619–623*.
- (59) Bauer, B. J.; Fetters, L. J.; Hadjichristidis, N.; Roovers, J. E. L. Star-Branched Polymers. 5. The θ Temperature Depression for 8- and 12-Arm Polyisoprenes in Dioxane. *J. Am. Chem. Soc.* **1980**, *102* (7), 2410–2413.
- (60) Suzuki, J.; Takano, A.; Matsushita, Y. Dimensions of Catenated Ring Polymers in Dilute Solution Studied by Monte-Carlo Simulation. *J. Chem. Phys.* **2018**, *149* (20), 204901.
- (61) Thompson, A. P.; Aktulga, H. M.; Berger, R.; Bolintineanu, D. S.; Brown, W. M.; Crozier, P. S.; in't Veld, P. J.; Kohlmeyer, A.; Moore, S. G.; Nguyen, T. D.; Shan, R.; Stevens, M. J.; Tranchida, J.; Trott, C.; Plimpton, S. J. LAMMPS a Flexible Simulation Tool for Particle-Based Materials Modeling at the Atomic, Meso, and Continuum Scales. *Comput. Phys. Commun.* 2022, 271, No. 108171.
- (62) Kremer, K.; Grest, G. S. Dynamics of Entangled Linear Polymer Melts: A Molecular-Dynamics Simulation. *J. Chem. Phys.* **1990**, 92 (8), 5057–5086.
- (63) Jung, Y.; Hyeon, C.; Ha, B. Y. Near- θ Polymers in a Cylindrical Space. *Macromolecules* **2020**, 53 (7), 2412–2419.
- (64) Liu, L.; Pincus, P. A.; Hyeon, C. Compressing θ -Chain in Slit Geometry. *Nano Lett.* **2019**, 19 (8), 5667–5673.
- (65) Wang, Z. G. 50th Anniversary Perspective: Polymer Conformation A Pedagogical Review. *Macromolecules* **2017**, *50* (23), 9073–9114.
- (66) Steinhauser, M. O. A Molecular Dynamics Study on Universal Properties of Polymer Chains in Different Solvent Qualities. Part I. A Review of Linear Chain Properties. *J. Chem. Phys.* **2005**, 122 (9), No. 094901.
- (67) Rudnick, J.; Gaspari, G. The Shapes of Random Walks. Science 1987, 237 (4813), 384–389.
- (68) Šolc, K. Shape of a Random-Flight Chain. J. Chem. Phys. 1971, 55 (1), 335–344.
- (69) Pakula, T.; Jeszka, K. Simulation of Single Complex Macromolecules. 1. Structure and Dynamics of Catenanes. *Macromolecules* 1999, 32 (20), 6821–6830.
- (70) Hegde, G. A.; Chang, J. F.; Chen, Y. L.; Khare, R. Conformation and Diffusion Behavior of Ring Polymers in Solution: A Comparison between Molecular Dynamics, Multiparticle Collision Dynamics, and Lattice Boltzmann Simulations. *J. Chem. Phys.* **2011**, 135 (18), 184901.
- (71) Bohn, M.; Heermann, D. W.; Lourenço, O.; Cordeiro, C. On the Influence of Topological Catenation and Bonding Constraints on Ring Polymers. *Macromolecules* **2010**, 43 (5), 2564–2573.
- (72) Li, B.; Madras, N.; Sokal, A. D. Critical Exponents, Hyperscaling, and Universal Amplitude Ratios for Two- and Three-Dimensional Self-Avoiding Walks. *J. Stat. Phys.* **1995**, *80* (3–4), *661*–754.
- (73) Grassberger, P.; Hegger, R. Simulations of Three-Dimensional θ Polymers. *J. Chem. Phys.* **1995**, 102 (17), 6881–6899.